Combined Effects of Geometric Rotation and Antenna Calibration Patterns on GNSS Phase Windup

Jason H. Rife[1], *Member, IEEE*, Brandon Weaver[1], Tony Bogner[2], and J. Arnold Soltz[2]

Abstract—This paper examines GNSS phase windup, which we define to be the combined effects of three-dimensional rotation and antenna phase patterns on carrier-phase measurements. Specifically, phase windup equations are presented for antennae with spatially varying phase patterns, for instance phase patterns defined as a function of the satellite line-of-sight direction, as might be characterized by azimuth and zenith angles. We observe that a description both of the geometric rotation and also of the antenna phase pattern are needed to accurately evaluate phase windup for a general antenna. Furthermore, we show that there is not a unique approach for computing phase windup; in fact, correctly computing phase windup requires adjusting the model to match the calibration method used to obtain the antenna phase pattern.

Keywords: GNSS, Phase windup, Rotation, Calibration

I. Introduction

It is widely understood that GNSS carrier-phase measurements are influenced both by the relative range and by the relative rotation between the receive and transmit antennae. The term *phase windup* is commonly used to describe these rotation-dependent effects. Modeling phase-windup is particularly important for real-time kinematic (RTK) and precise-point positioning (PPP) applications [1]-[3], as well as for standalone applications involving dynamic platforms such as spacecraft [4],[5]. In some precision applications, two receive antennae are used differentially to remove phase windup effects [6]-[8]. In other applications, a single antenna is used so that rotational effects can be exploited to observe orientation or angular velocity [9]-[12].

For the vast majority of GNSS applications, phase windup can either be neglected or modeled simply. This paper considers the specific case of using an innovative antenna on a platform, such as a spacecraft or an aircraft, that rotates in three dimensions. Tools for modeling phase windup in these applications are not yet well developed in the research literature. At present, for example, it is possible to run an RF simulator using a known antenna pattern, but it is not trivial to program the simulator to account for phase windup in three dimensions.

Phase windup effects are the result of the interaction between a circularly polarized signal and the receive antenna. GNSS signals are designed to be right-hand circularly polarized (RHCP), but it is important to note that GNSS transmitters also create a small left-hand circularly polarized (LHCP) component along lines-of-sight (LOS) away from the *boresight axis*, which is the name given to the primary transmission axis of the antenna. It is useful to visualize the RHCP signal as a helix traveling through space and rotating around the boresight axis. The wrapping of the helix represents a steady progression of the signal's reference phase, which is in turn observed by the GNSS receiver. The reference phase increases with range from transmitter to receiver; however, the reference phase also increases if the receive antenna spins in the same sense as the helix. It is as if rotation and translation motions are coupled, at least in the sense that they are indistinguishable from the receiver's point of view.

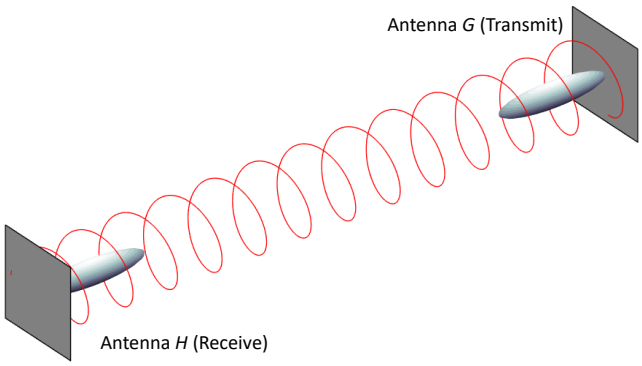

Fig. 1. Vizualization of a right-hand circularly polarized signal

A key detail is that phase windup results from interactions of an electric field with the receive antenna. As such, it is intuitive that any general model of phase windup must be related to both geometric rotation and to the antenna phase pattern, which we will also call the *antenna calibration pattern* in this paper. For simple antenna designs, phase windup may be dominated by purely geometric effects as modeled, for instance, in the seminal paper by Wu *et al.* [13]. Nonetheless, the purely geometric analysis of Wu is only an approximation, albeit a good one, as pointed out by Beyerle [14]. The Beyerle paper observed that, when the receive and transmit antennae are both idealized RHCP

[1] Dept. of Mechanical Engineering, Tufts University, Medford, MA, USA.
[2] The Charles Stark Draper Laboratory, Inc. Cambridge, MA, USA.

crossed-dipoles, the phase windup depends on the full antenna phase pattern (including both RHCP and LHCP components) if the LOS axis is tilted significantly from the boresight axes of both antennae.

The paper by Beyerle emphasizes the relevance of modeling phase windup as the combined result of geometric rotations and antenna calibration patterns; however, the paper stops short of developing approaches for analyzing general calibration patterns. To be specific, [14] considers only crossed-dipole antennae; moreover, the antenna model considered was a three-dimensional (3D) complex vector. This approach of describing the antenna gain pattern as a complex vector is common in computational packages that solve Maxwell's equations [15] and in antenna theory textbooks [16],[17]; however, GNSS practitioners more commonly model antenna calibration patterns as complex scalar functions defined over two dimensions (e.g. over azimuth/elevation or azimuth/zenith coordinates) [18]-[24].

The primary goal of this paper is to address this gap by adapting phase windup models to account for arbitrary calibration patterns. In the process we note that different techniques can be used to obtain an antenna calibration and, accordingly, that the phase windup model must be matched specifically to the calibration method used.

The remainder of the paper is organized as follows. First, we develop a measurement model for carrier phase that accounts for windup. Second, we discuss methods for representing the antenna calibration pattern. Third, we review equations for relating phase windup to geometric rotation. Next, we outline two different approaches for calibration of the antenna pattern, noting that each results in a different equation for phase windup. The paper closes with a simulation-based evaluation of the equations presented in the paper and a brief conclusion.

II. Measurement Model

This section reviews modeling of the carrier-phase measurement, which is well characterized in the existing literature, for example in [1] and [25]. The carrier-phase measurement is commonly used to infer the true range $r_{H/G}$ between reference points, from point *G* on the satellite antenna to point *H* on the receive antenna. For this reason, the carrier-phase Φ is sometimes reported in length units; however, in this paper, we will model Φ in radian units. Thus, the range dependency must be converted to radian units by a factor $\frac{2\pi}{\lambda}$, where λ is the carrier wavelength. Carrier-phase also depends on clock bias *b*, tropospheric delay *T*, and ionospheric delay *I*, terms which are also typically expressed in range units and which must be scaled accordingly, as in the following expression modeling the carrier-phase measurement.

$$\Phi = \frac{2\pi}{\lambda}\left(r_{H/G} + b + T - I\right) + 2\pi N + \alpha + \beta + \eta \qquad (1)$$

The remaining terms in the model are expressed in radian units. The first term after the parentheses is the ambiguity $N\lambda$, where *N* is an integer. Other terms include the antenna correction α, which accounts for phase windup including the effects of the antenna calibration pattern; the moment-arm term β, which accounts for phase offset due to the displacement of the antenna phase center when rotated about a designated reference point; and the measurement noise term η.

If the receive antenna is static, then rotations (e.g. due to the satellite's orbit about the Earth) are slow, and both the α and β terms can be estimated as unmodeled drift in the clock term b. However, if the receive antenna is rotating rapidly, then it is useful to expand the models for α and β in more detail, as both are sensitive to rotation.

A. Antenna Correction α

The antenna correction can be modeled concisely [13],[14] as a dot product of the complex gain vectors **G** and **H**, which describe the calibration patterns of the transmit and receive antennae, respectively:

$$\alpha = \angle \mathbf{G} \cdot \mathbf{H} + 2\pi M. \qquad (2)$$

The dot product of the two gain patterns is a complex scalar, from which the phase angle is extracted by the angle operator $\angle$. The range of the operator is $(-\pi, \pi)$, but α can take any real value: $\alpha \in (-\infty, \infty.)$ The antenna ambiguity *M* is introduced to reconcile the difference by accounting for α wrapping outside the range of the angle operator.

Notably, the variable names **G** and **H** represent a somewhat nonstandard notation for the vector gain patterns of the transmit and receive antennae. By contrast, a typical GNSS link budget might use subscripts to distinguish between antennae (e.g. a *T* subscript for transmit and an *R* subscript for receive). To maintain a compact mathematical notation in this paper, we instead use subscripts to identify different coordinate systems. To avoid overloading subscripts, we use different variable names (rather than subscripts) for distinguishing the receiver and transmitter gain patterns. The letter **H** was chosen for the receive antenna because it is sequential. (**G** comes before **H** in the alphabet, just as transmitter comes before receiver in radio navigation.) Conveniently, our approach in this paper does not require analysis of a magnetic field (commonly denoted as **H** in the electromagnetics literature), which leaves the variable **H** available to describe the receive antenna.

In this paper, our goal will be to transform the vector patterns **G** and **H** into scalar patterns describing antenna response to RHCP and LHCP components of the received signal, as the latter form is commonly used in GNSS analyses. To appreciate the distinction, it is useful to briefly summarize the derivation of (2). First, the electric field in the vicinity of the receiver is modeled as an oscillating function in time, with a reference phase set by (1), excluding the antenna correction α:

$$\mathbf{E} = \sqrt{P}\mathbf{G}e^{j\left((\omega_c+\omega_d)t+\Phi-\alpha\right)}. \qquad (3)$$

Here *P* is power, **G** is the vector antenna calibration pattern for the transmit antenna, ω_c is the carrier frequency, and ω_d is the

Doppler shift. The vector **G** is a complex function, reflecting phase shift and amplitude scaling as a function of the LOS direction from the transmitter to receiver.

If a far-field assumption is made, implying that the receive and transmit antennae are separated by a long distance, then the electric field E has planar wavefronts at the receiver, and the receive antenna's output voltage can be modeled as

$$v = (\mathbf{G} \cdot \mathbf{H})\sqrt{P}e^{j(\Phi-\alpha)}e^{j(\omega_c+\omega_d)t}. \quad (4)$$

This equation introduces **H**, the vector calibration pattern for the receive antenna. For now we assume **H** is defined about the phase center rather than about some other reference point on the receive antenna (but we will relax this assumption shortly by introducing β, below).

The antenna correction term is the phase of the dot product in (4). If we introduce a variable D to describe the dot product's magnitude, we have

$$\mathbf{G} \cdot \mathbf{H} = De^{j\alpha}, \quad (5)$$

and consequently

$$v = D\sqrt{P}e^{j\Phi}e^{j(\omega_c+\omega_d)t}. \quad (6)$$

When the GNSS receiver performs coherent integration to remove the last term of (6), the carrier-phase can be extracted as Φ. The key point here is that equation (2), which models the antenna correction term α, is directly related to the vector dot product that modulates the received signal, as described by (4).

B. Moment-Arm Term β

In physical terms, the carrier phase measurement should reflect translation between the phase centers of the receive and transmit antennas; however, the measurement equation (1) was intentionally framed in terms of reference points rather than phase centers, with the term β introduced to reconcile the difference. As this section will justify, the equation for β is

$$\beta = \frac{2\pi}{\lambda}\left(\mathbf{r}_{O/H} \cdot \hat{\mathbf{k}}\right), \quad (7)$$

where $\mathbf{r}_{O/H}$ represents the vector (sometimes called the *moment arm*) from the receive-antenna reference point H to the phase-center O. Note that capital italics are used here to indicate a physical point in space (in contrast with capital bold letters, which are used to represent vectors).

Before deriving (7), it is worth considering why a distinction might be made between a reference point and a phase center. One reason is that a given antenna may have multiple phase centers, one for each GNSS signal frequency (as shown in Fig. 2). Identifying a single reference point simplifies the process of combining GNSS measurements across frequencies. Another consideration is that the phase center may lie in empty space, outside the antenna housing (see Fig. 2). Specifying a reference point at a physical location on the device, such as at the center of the electronics package (called *mechanical phase center* in [27]) or at the mounting point, clarifies interpretation of the carrier measurement. In fact, to support general sensor fusion, it may even be preferable to locate the reference point on a structure rigidly attached to the antenna (e.g. at the center-of-mass of a vehicle). For all these reasons, the measurement equation (1) refers to reference points rather than phase centers.

As defined above, the vector $\mathbf{r}_{O/H}$ describes the relative position of the receive-antenna phase center O to its reference point H. For simplicity, let us assume the phase center and reference point for the transmit antenna are collocated at G. In this case, the carrier measurement should depend on the length of the vector $\mathbf{r}_{O/G}$, from G to O. By vector addition [26]:

$$\mathbf{r}_{O/G} = \mathbf{r}_{O/H} + \mathbf{r}_{H/G}. \quad (8)$$

More precisely, the carrier measurement depends only on the vector's magnitude, which can be obtained by dotting (8) with $\hat{\mathbf{k}}$, the unit vector in the LOS direction from G to H:

$$\hat{\mathbf{k}} = \frac{\mathbf{r}_{H/G}}{\|\mathbf{r}_{H/G}\|}. \quad (9)$$

When the moment arm is much shorter than the distance between receiver and transmitter, the LOS vector is essentially the same to both points O and H, and hence it is a very reasonable approximation to write $\hat{\mathbf{k}} \approx \mathbf{r}_{O/G}/\|\mathbf{r}_{O/G}\|$. Applying this approximation and dotting (8) with $\hat{\mathbf{k}}$ gives:

$$r_{O/G} = \mathbf{r}_{O/H} \cdot \hat{\mathbf{k}} + r_{H/G}. \quad (10)$$

Substituting (7) into (1), then combining range terms with (10), gives:

$$\Phi = \frac{2\pi}{\lambda}\left(r_{O/G} + b + T - I\right) + 2\pi N + \alpha + \eta. \quad (11)$$

This equation is equivalent to (1) except in that it makes explicit the underlying physics that relate the carrier phase measurement to the location of the receive-antenna phase center O. The utility of the original equation (1), as compared to (11), is that the former allows for an arbitrary receive-antenna reference point.

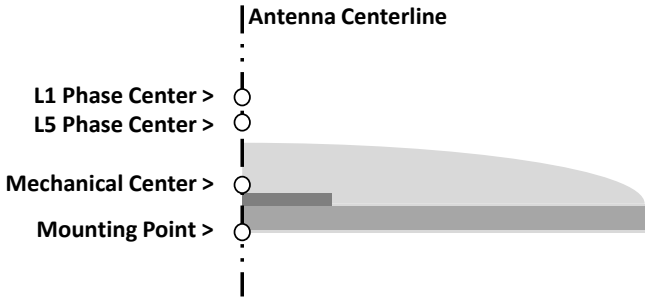

Fig. 2. Representative phase centers for a GNSS antenna, adapted from [27]. In this special case, the phase centers are collinear and happen to lie outside the physical extent of the antenna.

The form of the moment-arm correction term β is intentionally made similar to that of the phase windup term α, since the gain-pattern may be calibrated for an arbitrary reference point (such that the reported pattern is actually the sum $\alpha + \beta$).

III. Antenna Models

This section represents the key contribution of the paper, in that it introduces a method to convert the antenna calibration pattern from a vector field, like **G** or **H**, into a scalar field defined over all possible LOS. This conversion is significant because phase windup is most precisely described using a vector gain pattern, yet manufacturers most often specify the gain pattern as a scalar field (e.g., a function of azimuth and elevation angle) since scalar-field gain patterns are much easier to use when the antenna is stationary. The conversion is implemented using a change of coordinates, which we will introduce and then subsequently illustrate using a canonical example: the case of the RHCP crossed-dipole antenna.

A. Coordinate Systems

Quantifying the vector gain patterns **G** and **H** requires a coordinate system. In this paper, we use Cartesian coordinates fixed to an antenna where the z-direction is aligned with the boresight axis in the direction of signal travel. In other words, the z-direction is outward along the boresight for the transmit antenna and inward along the boresight for the receive antenna; this choice simplifies later math, because the antenna-fixed bases for the receive and transmit antennae are aligned when the antennae are in their nominal configuration, as shown in Fig. 3. The x-axis and y-axis are defined as orthogonal vectors in the plane perpendicular to the boresight axis, which is the ground plane for some antennae. Label the orthonormal set of basis vectors fixed to the transmit antenna as $\{\hat{\mathbf{g}}_x, \hat{\mathbf{g}}_y, \hat{\mathbf{g}}_z\}$ and the set fixed to the receive antenna as $\{\hat{\mathbf{h}}_x, \hat{\mathbf{h}}_y, \hat{\mathbf{h}}_z\}$.

GNSS systems use RHCP signals, meaning that the phase on the $\hat{\mathbf{g}}_x$ axis leads the phase on the $\hat{\mathbf{g}}_y$ axis by 90°. The transmitted signal is right handed in the sense that it travels in the $\hat{\mathbf{g}}_z$ direction while corkscrewing around that axis, curling in the direction of the fingers on a right hand with its thumb pointed in the $\hat{\mathbf{g}}_z$ direction. For the nominal configuration, with the receive and transmit antennae aligned, the arriving signal is also right-handed about the receive-antenna's $\hat{\mathbf{h}}_z$ axis.

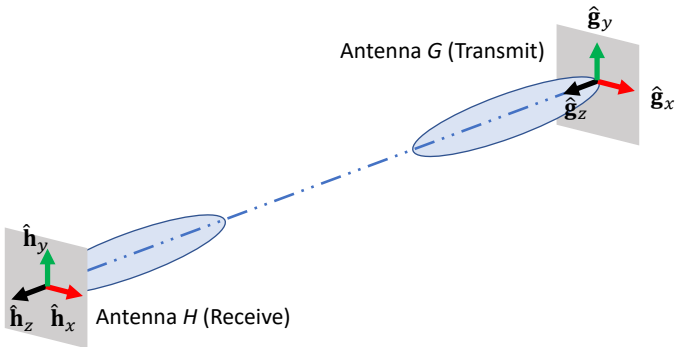

Fig. 3. Cartesian basis vectors for transmitter and receiver. The z-axis aligns with each antenna's boresight (in the direction of intended signal travel); the x-axis leads the y-axis in the right-hand sense.

In Cartesian coordinates, a circularly polarized signal can be described using complex numbers, where the imaginary number j represents a 90° phase lead and its negative ($-j$) represents a 90° phase lag. Thus, an RHCP basis vector with unit magnitude can be written $\hat{\mathbf{g}}_R = \frac{1}{\sqrt{2}}\left(\hat{\mathbf{g}}_x - j\hat{\mathbf{g}}_y\right)$, and an LHCP basis vector can be written similarly. Because the component of the electric field is always zero parallel to the LOS vector $\hat{\mathbf{k}}$, however, the LHCP and RHCP basis vectors must be constructed carefully by first rotating into a coordinate system where the x-axis and y-axis are defined to be orthogonal to $\hat{\mathbf{k}}$. For this purpose, introduce intermediate bases $\{\hat{\mathbf{g}}'_x, \hat{\mathbf{g}}'_y, \hat{\mathbf{k}}\}$ and $\{\hat{\mathbf{h}}'_x, \hat{\mathbf{h}}'_y, \hat{\mathbf{k}}\}$, which are fixed to the transmit and receive antennae respectively. Since the associated x and y-vectors for the transmitter are orthogonal to the LOS, a polarization basis can now be defined:

$$\begin{aligned}\hat{\mathbf{g}}'_R &= \frac{1}{\sqrt{2}}\left(\hat{\mathbf{g}}'_x - j\hat{\mathbf{g}}'_y\right)\\ \hat{\mathbf{g}}'_L &= \frac{1}{\sqrt{2}}\left(\hat{\mathbf{g}}'_x + j\hat{\mathbf{g}}'_y\right)\end{aligned} \tag{12}$$

A similar transformation can be defined for the receiver. The result is a pair of polarization bases, $\{\hat{\mathbf{g}}'_R, \hat{\mathbf{g}}'_L, \hat{\mathbf{k}}\}$ and $\{\hat{\mathbf{h}}'_R, \hat{\mathbf{h}}'_L, \hat{\mathbf{k}}\}$, the first for the transmitter and the second for the receiver. These intermediate bases are illustrated in Fig. 4, which shows a configuration where the boresight directions of the antenna and receiver are not aligned.

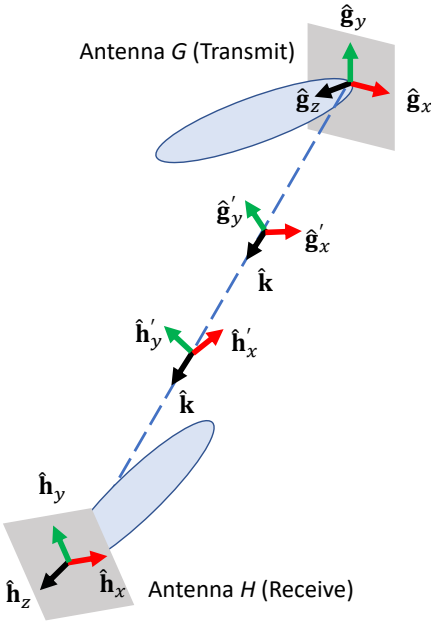

Fig. 4. Antenna geometry for an arbitrary LOS vector $\hat{\mathbf{k}}$

With the polarization bases defined, it is now possible to describe any vector in polarization coordinates. For instance, the transmitter's vector antenna pattern $\mathbf{G}$ can be transformed into a coordinate pair (p,q) by dotting with the associated polarization basis vectors.

$$\begin{aligned} p &= \hat{\mathbf{g}}'_R \cdot \mathbf{G} \\ q &= \hat{\mathbf{g}}'_L \cdot \mathbf{G} \end{aligned} \tag{13}$$

The third component is always zero ($\hat{\mathbf{k}} \cdot \mathbf{H} = \hat{\mathbf{k}} \cdot \mathbf{G} = 0$), since the electric field is planar.

The receiver's vector antenna pattern $\mathbf{H}$ can likewise be transformed into a coordinate pair (r,s).

$$\begin{aligned} r &= \hat{\mathbf{h}}'_R \cdot \mathbf{H} \\ s &= \hat{\mathbf{h}}'_L \cdot \mathbf{H} \end{aligned} \tag{14}$$

Equivalently, the polarization coordinates can be written in matrix form as

$$\begin{bmatrix} p \\ q \\ 0 \end{bmatrix} = \left[{}^{p}\mathbf{U}^{c} \right] \left[{}^{G'_c}\mathbf{R}^{G_c} \right] [\mathbf{G}]_{G_c} \tag{15}$$

and

$$\begin{bmatrix} r \\ s \\ 0 \end{bmatrix} = \left[{}^{p}\mathbf{U}^{c} \right] \left[{}^{H'_c}\mathbf{R}^{H_c} \right] [\mathbf{H}]_{H_c}. \tag{16}$$

These equations rely on a unitary matrix ${}^{p}\mathbf{U}^{c}$ converting between Cartesian and polarization coordinates as well as a pair of rotation matrices, $\left[{}^{G'_c}\mathbf{R}^{G_c} \right]$ and $\left[{}^{H'_c}\mathbf{R}^{H} \right]$. The first of these rotation matrices maps from G_c , which refers to the transmitter boresight-aligned basis $\{\hat{\mathbf{g}}_x, \hat{\mathbf{g}}_y, \hat{\mathbf{g}}_z\}$, to G'_c, which refers to the transmitter LOS-aligned basis $\{\hat{\mathbf{g}}'_x, \hat{\mathbf{g}}'_y, \hat{\mathbf{k}}\}$. Similarly, the second rotation matrix maps from the receiver boresight-aligned to the receiver LOS-aligned basis, meaning from $\{\hat{\mathbf{h}}_x, \hat{\mathbf{h}}_y, \hat{\mathbf{h}}_z\}$ to $\{\hat{\mathbf{h}}'_x, \hat{\mathbf{h}}'_y, \hat{\mathbf{k}}\}$.

As for the unitary matrix ${}^{p}\mathbf{U}^{c}$, let us start by defining its inverse ${}^{c}\mathbf{U}^{p}$, which converts from polarization coordinates to Cartesian coordinates.

$${}^{c}\mathbf{U}^{p} = \frac{1}{\sqrt{2}} \begin{bmatrix} 1 & 1 & 0 \\ -j & j & 0 \\ 0 & 0 & \sqrt{2} \end{bmatrix}. \tag{17}$$

The columns of this matrix are simply the coefficients of (12) when the following dot products are evaluated:

$${}^{c}\mathbf{U}^{p} = \begin{bmatrix} \hat{\mathbf{g}}'_x \cdot \hat{\mathbf{g}}'_R & \hat{\mathbf{g}}'_x \cdot \hat{\mathbf{g}}'_L & \hat{\mathbf{g}}'_x \cdot \hat{\mathbf{k}} \\ \hat{\mathbf{g}}'_y \cdot \hat{\mathbf{g}}'_R & \hat{\mathbf{g}}'_y \cdot \hat{\mathbf{g}}'_L & \hat{\mathbf{g}}'_y \cdot \hat{\mathbf{k}} \\ \hat{\mathbf{k}} \cdot \hat{\mathbf{g}}'_R & \hat{\mathbf{k}} \cdot \hat{\mathbf{g}}'_L & \hat{\mathbf{k}} \cdot \hat{\mathbf{k}} \end{bmatrix}. \tag{18}$$

The inverse of this matrix is ${}^{p}\mathbf{U}^{c} = ({}^{c}\mathbf{U}^{p})^{-1} = ({}^{c}\overline{\mathbf{U}}^{p})^{T}$, where the overbar in the last term indicates the complex conjugate. It is important to recall that when taking the transpose of a complex matrix (an operation also called the *Hermitian*), each complex entry of the transposed matrix should be conjugated. A conjugate transpose operation must be used to compute all dot products. Note that the dot products in (18) are straightforward to evaluate with (12), because the coefficients of the leading vector are real, so the conjugate operation has no effect.

B. Evaluating Antenna Phase Contribution α

The RHCP polarization coordinates r is what we seek to describe the antenna calibration pattern as a complex scalar field over all LOS directions. This section derives a relationship that uses the calibration pattern r to compute the antenna phase correction α, even when the receive antenna is rotating. To be general, we will also consider the LHCP component of the signal, which allows α to be computed even when the electrical field arriving at the receiver is elliptically polarized (meaning a mix of RHCP and LHCP components [17]).

To compute α in terms of polarization coordinates, we return to our fundamental equation (2), which expressed α as a dot product. Using matrices, the dot product can be evaluated as

$$\mathbf{G} \cdot \mathbf{H} = [\overline{\mathbf{G}}]^{T}_{G_c} \left[{}^{G_c}\mathbf{R}^{H_c} \right] [\mathbf{H}]_{H_c}. \tag{19}$$

The rotation matrix $\left[{}^{G_c}\mathbf{R}^{H_c} \right]$ converts from the receiver's boresight-aligned basis to the transmitter's boresight aligned basis. By substituting (15) and (16), we can expand (19).

$$\mathbf{G} \cdot \mathbf{H} = \begin{bmatrix} \bar{p} \\ \bar{q} \\ 0 \end{bmatrix}^{T} \left[{}^{p}\mathbf{U}^{c} \right] \left[{}^{G'_c}\mathbf{R}^{H'_c} \right] \left[{}^{p}\overline{\mathbf{U}}^{c} \right]^{T} \begin{bmatrix} r \\ s \\ 0 \end{bmatrix} \tag{20}$$

As desired, this equation has extracted the receive antenna pattern in terms of polarization coordinates (r,s). The expression also describes the local electric field in terms of polarization coordinates (p,q). To further simplify (20), we leverage a remarkable identity. If the rotation matrix $\left[{}^{G'_c}\mathbf{R}^{H'_c} \right]$ is written in terms of a single angle (i.e. the angle ψ from $\hat{\mathbf{g}}'_x$ to $\hat{\mathbf{h}}'_x$ about the common $\hat{\mathbf{k}}$ axis), then

$$\left[{}^{H'_c}\mathbf{R}^{G'_c} \right] = \left[{}^{G'_c}\mathbf{R}^{H'_c} \right]^{T} = \begin{bmatrix} \cos\psi & \sin\psi & 0 \\ -\sin\psi & \cos\psi & 0 \\ 0 & 0 & 1 \end{bmatrix} \tag{21}$$

and

$$\left[{}^{p}\mathbf{U}^{c} \right] \left[{}^{G'_c}\mathbf{R}^{H'_c} \right] \left[{}^{p}\overline{\mathbf{U}}^{c} \right]^{T} = \begin{bmatrix} e^{j\psi} & 0 & 0 \\ 0 & e^{-j\psi} & 0 \\ 0 & 0 & 1 \end{bmatrix} \tag{22}$$

Substituting into (20) gives

$$\mathbf{G} \cdot \mathbf{H} = \bar{p} r e^{j\psi} + \bar{q} s e^{-j\psi}. \tag{23}$$

The equation is a dot product in polarization coordinates, where the rotations between the two antennae are characterized by a spin angle ψ about the LOS axis. Computing α with (2), which extracts the phase angle from (23), we have

$$\alpha = \angle\left(\bar{p}re^{j\psi} + \bar{q}se^{-j\psi}\right) + 2\pi M. \tag{24}$$

Note that the pair (p,q) can be used to describe either the transmit antenna or the local electric field, since they are proportional (i.e. $\mathbf{E} = \gamma\mathbf{G}$, where γ is a real scalar).

For many GNSS applications where the LOS direction is nearly parallel to the transmitter boresight, and where the signal is nearly pure RHCP, we can further simplify. If the LHCP component is $q = 0$, then (24) becomes

$$q = 0 \;\rightarrow\; \alpha = \angle(\bar{p}r) + \psi + 2\pi M. \tag{25}$$

This equation clearly illustrates how both the gain pattern and geometric rotation impact α. In the pure RHCP case modeled by (25), the first term represents a correction due to the antenna phase pattern and the second term is simply proportional to the rotation angle about the LOS axis.

C. Crossed Dipole Antennae

To appreciate the difference between the antenna models in Cartesian and polarization coordinates, it is instructive to consider a canonical example, that of the RHCP crossed-dipole antenna. This antenna is the baseline for many studies modeling phase windup, including those of Wu [13] and Beyerle [14].

As reported by Beyerle, the Cartesian model of the RHCP crossed-dipole (evaluated about its phase center) can be computed for the transmitter pattern as

$$\mathbf{G} = C_g\left(\bar{\bar{\mathbf{I}}} - \hat{\mathbf{k}}\hat{\mathbf{k}}\right) \cdot \left(\hat{\mathbf{g}}_x - j\hat{\mathbf{g}}_y\right) \tag{26}$$

and for the receiver pattern as

$$\mathbf{H} = C_h\left(\bar{\bar{\mathbf{I}}} - \hat{\mathbf{k}}\hat{\mathbf{k}}\right) \cdot \left(\hat{\mathbf{h}}_x - j\hat{\mathbf{h}}_y\right). \tag{27}$$

Here C_g and C_h are arbitrary gains that do not affect phase angle calculations. The identity tensor is denoted $\bar{\bar{\mathbf{I}}}$. These expressions take an RHCP basis vector and remove the LOS component through the dot product with $\left(\bar{\bar{\mathbf{I}}} - \hat{\mathbf{k}}\hat{\mathbf{k}}\right)$, which is a projection operation.

Starting with these equations, we derived the corresponding equations in polarization coordinates, as detailed in Appendix A. The end result is that the equivalent expressions written in terms of (p,q) for the transmitter and (r,s) for the receiver are

$$\begin{bmatrix} p \\ q \end{bmatrix} = \frac{C_g}{\sqrt{2}}\begin{bmatrix} \cos Z_g + 1 \\ \left(\cos Z_g - 1\right)e^{-j2A_g} \end{bmatrix} \tag{28}$$

and

$$\begin{bmatrix} r \\ s \end{bmatrix} = \frac{C_h}{\sqrt{2}}\begin{bmatrix} \cos Z_h + 1 \\ \left(\cos Z_h - 1\right)e^{-j2A_h} \end{bmatrix}. \tag{29}$$

Here (A_g, Z_g) are the Azimuth and Zenith angle of the LOS vector $\hat{\mathbf{k}}$ relative to the transmitter basis $\left\{\hat{\mathbf{g}}_x, \hat{\mathbf{g}}_y, \hat{\mathbf{g}}_z\right\}$, and (A_h, Z_h) are the Azimuth and Zenith angle of the LOS vector $\hat{\mathbf{k}}$ relative to the receiver basis $\left\{\hat{\mathbf{h}}_x, \hat{\mathbf{h}}_y, \hat{\mathbf{h}}_z\right\}$. If the derivation is correct, we expect that the Cartesian models (26) and (27) and the polarization-coordinate models (28) and (29) should produce the same phase correction α. This verification test will be evaluated in Section VI.

An important detail here is that equations (28) and (29) are representative of how calibration patterns are often represented for physical hardware. This is to say, even when a closed form model is not available, antennae are often calibrated to produce a phase-correction surface as a function of an Azimuth/Zenith or an Azimuth/Elevation angle pair, with the form $r(A_h, Z_h)$. In some cases, these surfaces are represented with a lookup table, in other cases they are represented with a polynomial fit or with spherical harmonics [20].

IV. LOS Rotation Angle

In order to use polarization coordinates to compute α using (24), the missing detail is to evaluate the spin angle ψ about the LOS axis. This section reviews two such methodologies, both of which are drawn from the existing literature.

A. Euler Angle Method

Three-dimensional (3D) rotations are often characterized using Euler angles [26]. A set of Euler angles consists of three scalar angles defined about three specified axes. For antenna characterization, it is most convenient to consider a set of Body ZYZ Euler angles, where two rigid bases are related by rotation angles defined sequentially about the z-axis, y-axis, and z-axis of the second basis.

The orientation of the receiver relative to the transmitter can be decomposed into two successive 3D rotations, one relating an intermediate basis L to the transmitter basis G, and a second relating the receiver basis H to the common intermediate basis L. The intermediate basis L is defined to align with the LOS vector, and consists of orthonormal basis vectors $\left\{\hat{\mathbf{i}}, \hat{\mathbf{j}}, \hat{\mathbf{k}}\right\}$. The vectors $\hat{\mathbf{i}}$ and $\hat{\mathbf{j}}$ can be selected as any vector pair for which $\hat{\mathbf{j}} = \hat{\mathbf{k}} \times \hat{\mathbf{i}}$. From these basis vectors, the rotation matrix ${}^{L}\mathbf{R}^{G}$ can be created to map from $\left\{\hat{\mathbf{g}}_x, \hat{\mathbf{g}}_y, \hat{\mathbf{g}}_z\right\}$ to $\left\{\hat{\mathbf{i}}, \hat{\mathbf{j}}, \hat{\mathbf{k}}\right\}$. Similarly, the rotation matrix ${}^{H}\mathbf{R}^{L}$ can be created to map from $\left\{\hat{\mathbf{i}}, \hat{\mathbf{j}}, \hat{\mathbf{k}}\right\}$ to $\left\{\hat{\mathbf{h}}_x, \hat{\mathbf{h}}_y, \hat{\mathbf{h}}_z\right\}$. If the Body ZYZ angles for ${}^{L}\mathbf{R}^{G}$ are defined to be $\{\phi_1, \phi_2, \phi_3\}$ and if the Body ZYZ angles for ${}^{L}\mathbf{R}^{H}$ are defined to be $\{\theta_1, \theta_2, \theta_3\}$, then the LOS spin angle can be written :

$$\psi = \phi_1 + \phi_3 - \theta_1 - \theta_3. \tag{30}$$

This result is obtained from [13] as explained in Appendix B.

Although Euler angles are useful for mathematical analysis, they pose a number of difficulties for numeric implementation, including non-uniqueness, singularities, and a need to evaluate computationally intensive inverse-trigonometric functions. To streamline numeric implementation, an alternative vector-based approach is desired to obtain ψ.

B. Effective Dipole Method

A vector-based method for extracting the LOS rotation angle ψ is the effective dipole approach [5],[13]. Importantly, this approach is computationally efficient and singularity free. The idea is to define two "effective" (linearly polarized) dipoles oriented perpendicular to the boresight axes of the transmit and receive antennae. The effective dipoles are:

$$\mathbf{D}_g = \hat{\mathbf{g}}_x - \hat{\mathbf{k}}\left(\hat{\mathbf{k}} \cdot \hat{\mathbf{g}}_x\right) - \mathbf{k} \times \hat{\mathbf{g}}_y. \tag{31}$$

and

$$\mathbf{D}_h = \hat{\mathbf{h}}_x - \hat{\mathbf{k}}\left(\hat{\mathbf{k}} \cdot \hat{\mathbf{h}}_x\right) - \mathbf{k} \times \hat{\mathbf{h}}_y. \tag{32}$$

These effective dipoles can be used to compute ψ as

$$\psi = \text{atan2}\left(\mathbf{k} \cdot \left(\mathbf{D}_g \times \mathbf{D}_h\right), \mathbf{D}_g \cdot \mathbf{D}_h\right). \tag{33}$$

V. Calibration

This section revisits the antenna gain pattern, to consider how the LOS rotation angle ψ plays into the calibration process. The key contribution of this section is to demonstrate that the antenna calibration pattern is not unique, and that the baseline phase correction model (24) must be modified if the calibration procedure induces spin.

In order to demonstrate this point, we consider two calibration procedures. In the first procedure, we assume that each LOS direction is sampled using a three-axis rotation stage, which performs a Body ZYZ rotation on the receive antenna; in the second procedure, we assume a two-axis rotation stage, which performs a Body ZY rotation. Both procedures produce a calibration surface over a range of Azimuth and Zenith angles; however, the calibration surfaces will not necessarily agree.

In analyzing these two procedures, we assume all other details are the same other than the process for rotating the receive antenna. Importantly, we assume calibration in an anechoic chamber with high carrier-to-noise ratio, such that measurement noise and multipath errors are negligibly small. We assume rotations occur about the same reference point for both rotation stages. We assume that the receive antenna is sufficiently far from the transmit antenna that a far-field assumption is justified. Also, we assume that the transmitter can be configured either with an RHCP or with an LHCP antenna, to transmit a purely circularly polarized signal such that r and s can be calibrated separately. In other words, we assume that the RHCP calibration surface is measured in an electric field with $(p,q) = (1,0)$ and the LHCP surface, with $(p,q) = (0,1)$. Finally, we assume that the calibration is referenced to a neutral configuration, in which the basis vectors for the transmitter and receiver are aligned, as shown in Fig. 3.

A. Body ZYZ Calibration

First consider the Body ZYZ calibration procedure. This procedure uses three rotation stages even though, technically, only two stages are needed to cover all azimuth and zenith angles describing the LOS direction. The redundant angle can be used to remove spin introduced by rotating the receive antenna through to any given azimuth. This is to say, the Euler angle set $\{\theta_1, \theta_2, \theta_3\}$ used to rotate the receive antenna relative to the test chamber is opposite to the azimuth and zenith angles that describe the rotation of the LOS vector $\hat{\mathbf{k}}$ relative to the antenna boresight-fixed basis:

$$A_h = -\theta_1 \text{ and } Z_h = -\theta_2. \tag{34}$$

Manipulating (30) to ensure that ψ is constant, we see the third rotation stage should configured such that $\theta_3 = -\theta_1 = A_h$.

The calibration procedure then progresses through a predefined sequence of motions to sample the carrier-phase in a pure RHCP field at all relevant azimuth-zenith pairs, to give $\rho_R(A_h, Z_h)$. Here the R subscript refers to RHCP calibration, where the alternative is an L subscript referring to the LHCP calibration. If phase is tracked continuously during the calibration process, then each sample can be differenced from the initial sample acquired when the antennas are aligned. The initial samples for the RHCP and LHCP tests are ρ_{R0} and ρ_{L0}, respectively.

Subtracting the initial measurement removes many confounding effects and helps to reveal the desired calibration pattern. It is evident from (1) that all terms are removed in the test except for the clock b, which may drift over time, and the antenna correction α, which is needed for the calibration process. Note that the moment-arm β is effectively zero, since we assume the rotation stage rotates about the desired reference point on the antenna.

If clock drift can be removed, either by using a common clock for both receiver and transmitter or by estimating clock drift separately, then the measurement difference directly reveals the antenna phase shift relative to the neutral configuration. For the RHCP data collection run, for instance, we can write:

$$\rho_R(A_h, Z_h) - \rho_{R0} = \alpha(A_h, Z_h) - \alpha(0,0). \tag{35}$$

Further simplification is possible if we recognize that, for a pure RHCP signal, the antenna phase α can be evaluated with (25). Since the LOS rotation angle ψ and the transmitter phase $\angle\bar{p}$ are constant throughout the experiment, the only terms that do not cancel in (35) are the receiver RHCP calibration $r(A_h, Z_h)$ and the integer M. If the calibration angle for the reference configuration $r(0,0)$ is set to be zero, then substituting (25) into (35) gives

$$\rho_R(A_h, Z_h) - \rho_{R0} = \angle r(A_h, Z_h) + 2\pi\Delta M. \quad (36)$$

where ΔM denotes the number of phase-wraps since the start of calibration. Leveraging this result, we can calibrate the RHCP phase pattern to be

$$r(A_h, Z_h) = \frac{D_R(A_h, Z_h)}{D_{R0}} \exp(j(\rho_R(A_h, Z_h) - \rho_{R0})). \quad (37)$$

This expression includes both phase and amplitude scaling, where the initial amplitude for the RHCP trial is D_{R0} and where each subsequent amplitude is $D_R(A_h, Z_h)$ forming a ratio that can be estimated, for example, from the signal-to-noise ratio. By analogy, a complex calibration surface can be derived for the LHCP trial to give

$$s(A_h, Z_h) = \frac{D_L(A_h, Z_h)}{D_{L0}} \exp(j(\rho_L(A_h, Z_h) - \rho_{L0})). \quad (38)$$

The terms in this equation for the LHCP analogs to the terms in (37). Together, (37) and (38) support online evaluation of the antenna correction via (24) in terms of the physical rotation of the antennae, as characterized by the LOS spin angle ψ.

B. Body ZY Calibration

Second consider the Body ZY calibration procedure. In this case, since the third Euler angle is fixed at zero, the LOS rotation ψ changes for each azimuth, with $\psi(A_h, Z_h) - \psi(0,0) = -\theta_1$, by (30). The resulting Body ZY antenna calibration gives two surfaces:

$$r^*(A_h, Z_h) = \frac{D_R(A_h, Z_h)}{D_{R0}} \exp(j(\rho_R(A_h, Z_h) - \rho_{R0})) \quad (39)$$

and

$$s^*(A_h, Z_h) = \frac{D_L(A_h, Z_h)}{D_{L0}} \exp(j(\rho_L(A_h, Z_h) - \rho_{L0})). \quad (40)$$

Here the star superscript is introduced to distinguish the Body ZY calibration from the prior results. Because the LOS spin angle is non-zero in the Body ZY, we can write the following equation to relate the starred variables back to the earlier values obtained by (37) and (38) for Body ZYZ calibration:

$$r^*(A_h, Z_h) = re^{-jA_h} \quad (41)$$

and

$$s^*(A_h, Z_h) = se^{+jA_h}. \quad (42)$$

The difference between the two calibrations is illustrated below in Fig. 5, which shows the calibration surfaces $r(A_h, Z_h)$ on the left and $r^*(A_h, Z_h)$ on the right.

Importantly, the antenna correction α given by (24) does compute the correct result for the Body ZY calibration surfaces r^* and s^*, unless the LOS spin angle is removed from (41) and (42) in post-processing. As an alternative, (24) can be reformulated by substituting (41) and (42) to give a Body ZY antenna correction equation:

$$\alpha = \angle\left(\overline{p^*}\, r^*\, e^{j\psi^*} + \overline{q^*}\, s^* e^{-j\psi^*}\right) + 2\pi M. \quad (43)$$

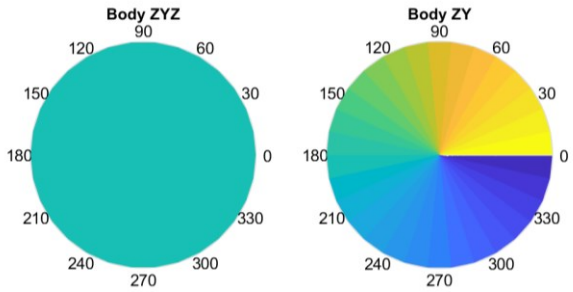

Fig. 5. Comparison of RHCP calibration surface for calibrations using a three-axis Body ZYZ rotation stage (left) and a two-axis Body ZY rotation stage (right). The color scale on the left plot ranges from π (yellow) to -π (dark blue).

Here the star notation is also added to the transmitter patterns p^* and q^* for consistency as well as the residual LOS rotation angle ψ^*, where this angle removes the azimuth (first Euler angles) contributions from (30) to give

$$\psi^* = \phi_3 - \theta_3. \quad (44)$$

A convenient formula for this angle correction is given in [13]:

$$\psi^* = \text{sign}\left(\hat{\mathbf{k}} \cdot \left(\hat{\mathbf{g}}'_y \times \hat{\mathbf{h}}'_y\right)\right) \text{acos}\left(\hat{\mathbf{g}}'_y \cdot \hat{\mathbf{h}}'_y\right). \quad (45)$$

Whether one of the two calibration strategies is "more correct" than the other is something of a philosophical question. In both cases, the phase windup α results from a combination of geometric rotation and antenna calibration; both approaches model these phenomena, and both are correct. The upshot is that there are multiple valid calibration approaches, each with its own formula for combining the calibrated phase pattern with a representation of geometric rotation to compute the phase correction α.

VI. Simulation

In this section we use simulation to verify the equations presented in this paper and explain their significance. To this end, we simulate the antenna phase correction α for several example cases.

In all simulation cases, the transmitter is fixed in space, as described by an inertially fixed basis $\{\hat{\mathbf{g}}_x, \hat{\mathbf{g}}_y, \hat{\mathbf{g}}_z\}$. The LOS vector $\hat{\mathbf{k}}$ is also inertially fixed, implying that the two antennae are offset but that they are not moving relative to one another. Except in the first case (which considers ideal circular polarization), the transmit antenna is modeled as an RHCP

crossed-dipole and the electric field is made elliptically polarized by tilting the LOS vector by 30° from the transmitter's boresight axis. Specifically, we set the LOS vector in the G basis to be $[\hat{\mathbf{k}}]_G = \begin{bmatrix} 0 & -\frac{1}{2} & \frac{\sqrt{3}}{2} \end{bmatrix}^T$.

The receive antenna is configured so that its basis vectors $\{\hat{\mathbf{h}}_x, \hat{\mathbf{h}}_y, \hat{\mathbf{h}}_z\}$ are initially aligned with those of the transmit antenna. In the simulation, the receive antenna is rotated one full rotation around a unit vector $\hat{\boldsymbol{\lambda}} = [-0.76 \quad 0.46 \quad 0.46]^T$. This rotation is illustrated in Fig. 6, which plots each LOS direction as a point on a unit sphere. In the figure, a signal arriving along the boresight of the receive antenna would be shown as a dot at the North pole. The actual LOS direction $\hat{\mathbf{k}}$ is initially offset 30° from the North pole (as indicated by a red half-circle). The trail of cyan dots shows each subsequent LOS direction $\hat{\mathbf{k}}$ as the receive antenna rotates about the $\hat{\boldsymbol{\lambda}}$ axis. The rotation axis $\hat{\boldsymbol{\lambda}}$ is depicted as a black arrow. During this rotation, the receive antenna sweeps through a wide range of zenith angles, including angles below the horizon, which is visualized as the "equator" of the unit sphere shown in Fig. 6.

For this geometric configuration, we consider four antenna models and evaluate α. The four models are summarized by Table 1. The models were selected to enable a new comparison with each model in the sequence.

A first comparison examines the effects of elliptical polarization. This comparison involves models (i) and (ii), which both assume an RHCP crossed-dipole receiver, but which assume a pure RHCP electric field in one case and an elliptically-polarized field in the other. The elliptically polarized electric field is generated by a crossed-dipole transmitter. In the pure RCHP case, the antenna phase shift is merely a geometric effect, described by (25); with elliptical polarization, the phase shift depends on both geometry and the antenna pattern, as described by the combination of equations (2), (26), and (27).

A second comparison verifies the equivalence of using Cartesian or polarization coordinates. We expect the two methods will be equivalent. To test this, we consider the RHCP crossed-dipole receive antenna subject to elliptical polarization. We compute α using a Cartesian vector formulation in model (ii) and then using polarization-coordinates in model (iii).

A final comparison illustrates how the polarization-coordinate formulation generalizes for analysis of general antenna patterns. For this case, we introduce a perturbed crossed-dipole, with a phase pattern that wraps in Azimuth, the result of adding an exponential term to the r component of conventional dipole antenna described by (29) to obtain:

$$\begin{bmatrix} r \\ s \end{bmatrix} = \frac{C_h}{\sqrt{2}} \begin{bmatrix} \cos Z_h + 1 \\ \cos Z_h - 1 \end{bmatrix} e^{-j2A_h} \tag{46}$$

This perturbed antenna is evaluated as model (iv); the effect of the perturbation can be assessed by comparison to the conventional RHCP crossed dipole evaluated as model (iii).

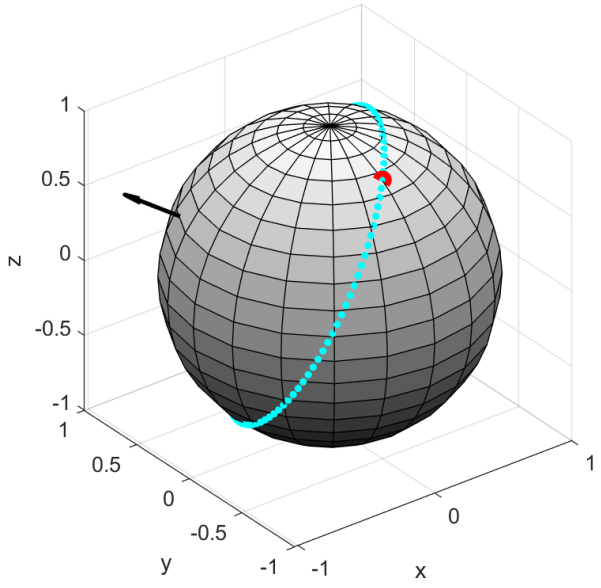

Fig. 6. LOS vector as seen by receive antenna. At each time step, the LOS vector $\hat{\mathbf{k}}$ is shown as a cyan point on the surface of a unit sphere. These points circle around the simple rotation axis (black arrow), starting at and returning to an initial orientation, which is marked as an open half-circle (red).

Table 1. Four models evaluated in simulation

ID	Electric field	Receiver	α equation
(i)	Pure RHCP	Crossed-dipole	(25), (30)
(ii)	Elliptically Polarized	Crossed-dipole (Beyerle model)	(2), (26), (27)
(iii)	Elliptically Polarized	Crossed-dipole (Polarization coord.)	(24), (28),(29)
(iv)	Elliptically Polarized	Perturbed crossed-dipole	(46)

This set of models represents a logical progression through the contributions of prior papers to the contributions of this paper. Wu's seminal paper [13] considered model (i), the case of a crossed-dipole receive antenna in a pure RHCP electric field. Beyerle's paper [14] considered model (ii), with the crossed-dipole receive antenna in an elliptically polarized electric field. By attempting to recreate Beyerle's results in polarization coordinates with model (iii), we verify that our generalized approach matches Beyerle for a canonical antenna (the RHCP crossed dipole). Our final case, that of model (iv), illustrates how our generalized approach extends to arbitrary antenna patterns.

The results of the simulation study conform to expectations. This is to say that the first two models of an RHCP crossed-dipole receiver (in pure RHCP and in elliptically polarized

fields, respectively) are expected to produce very similar results. Indeed, the computed phase shift values α are nearly identical for models (i) and (ii), as seen by comparing the red-dashed and blue-solid curves in Fig. 7. The two models only diverge substantially near a rotation of $\theta_\lambda = 3$ radians, where the LOS vector drops below the receiver's horizon. In this region, the LHCP component of the model becomes as large as the RHCP component, and the two models briefly diverge by as much as 0.67 radians (equivalent to 38° of phase shift).

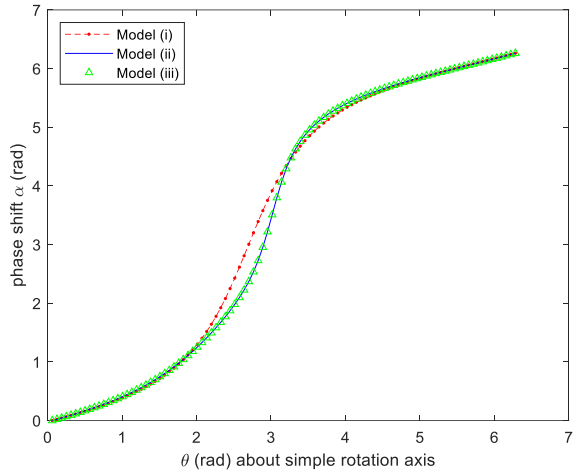

Fig. 7. Plot of total phase windup α as a function of the simple rotation angle θ_λ for models (i)-(iii). Both axes are reported in radian units.

Next, we can evaluate whether models (ii) and (iii) are equivalent, as we anticipated. Fig. 7 shows models (ii) and (iii) as the solid-blue curve and the green-triangle points; these two curves lie on top of each other within machine precision. This agreement shows that the proposed conversion between the two coordinate systems (Cartesian and polarization coordinates) is self-consistent, as expected.

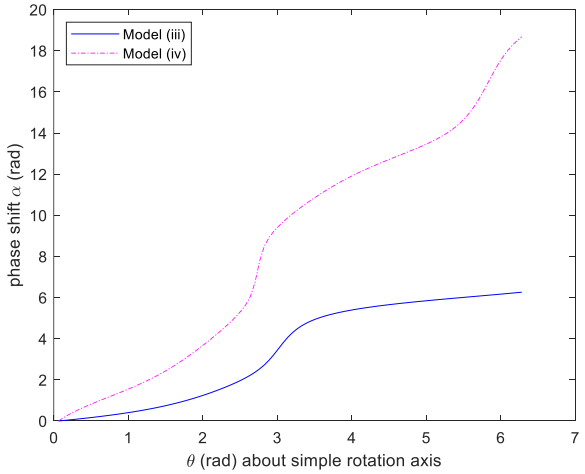

Fig. 8. Plot of total phase windup α as a function of the simple rotation angle θ_λ for conventional and perturbed antennae, labeled models (iii) and (iv).

The final comparison demonstrates the motivation for applying our proposed methodology when the receive antenna is not a crossed-dipole. To this end, consider α for the perturbed antenna of model (iv). The results from this model are compared to the conventional RCHP crossed-dipole, model (iii), in Fig. 8. In the figure, the crossed-dipole antenna is plotted as a solid-blue curve and the perturbed antenna, as a dashed-pink curve. The two antennae exhibit very different phase changes. During a physical rotation of one revolution ($\theta_\lambda = 2\pi$ rad) about the simple rotation axis, α for the conventional antenna changes by the same amount: 2π rad. The perturbed antenna has an entirely different behavior, with α changing by 6π rad for the same rotation. Clearly, this is a case in which both geometric rotation and antenna calibration must be considered together to accurately compute phase windup. As an aside, the high sensitivity of (46) to phase windup might be a disadvantage in some situations, but an advantage when attempting to infer attitude and angular velocity from phase angle measurements.

In order to enable other researchers to repeat and extend these studies, the Matlab simulation script that was used to generate Fig. 6 through Fig. 8 will be posted as an online supplement to this article.

VII. Conclusion

This paper builds on prior research on modeling GNSS phase windup. Our contribution is to introduce equations to account for the combined contributions of geometric rotation and antenna calibration to the carrier measurement; more specifically, we focus on calibration models formulated as complex scalar functions of two angles, such as the Azimuth and Zenith angles for the arriving signal. Simulations are used to check equation consistency. For reference, our Matlab-based simulation code is posted as an online supplement to this article.

In addition to presenting equations to model phase windup for general antennae, we demonstrate that calibration techniques are not all equivalent, and that the phase windup model equations must therefore be matched to the specific approach used to calibrate the antenna. As an example, we demonstrate the difference between calibrating an antenna with three rotation stages (Body ZYZ rotations) as opposed to only two rotation stages (Body ZY rotations).

The equations presented in this article are particularly relevant for aerospace platforms that rotate in three dimensions and that use nonstandard GNSS antennae. For such platforms, equations (24) and (33) can be used to describe combined phase windup effects in terms of both a lab-generated antenna calibration and rotations about the line-of-sight axis.

Acknowledgements

The authors gratefully acknowledge the Draper Fellowship Program and National Science Foundation grant CNS-1836942, which partially supported this research.

APPENDIX A

This Appendix derives the conversion of the RHCP crossed-dipole model from Cartesian coordinates to polarization coordinates. That is, we derive equations (28) and (29) from (26) and (27). To start our derivation, consider (26), which describes the pattern for the transmit antenna as a 3D vector, using a Cartesian basis:

$$\mathbf{G} = C_g\left(\bar{\bar{\mathbf{I}}} - \hat{\mathbf{k}}\hat{\mathbf{k}}\right) \cdot \left(\hat{\mathbf{g}}_x - j\hat{\mathbf{g}}_y\right) \tag{26}$$

Applying (13), which defines polarization coordinates, we have

$$\begin{aligned} p &= \hat{\mathbf{g}}'_R \cdot C_g\left(\bar{\bar{\mathbf{I}}} - \hat{\mathbf{k}}\hat{\mathbf{k}}\right) \cdot \left(\hat{\mathbf{g}}_x - j\hat{\mathbf{g}}_y\right) \\ q &= \hat{\mathbf{g}}'_L \cdot C_g\left(\bar{\bar{\mathbf{I}}} - \hat{\mathbf{k}}\hat{\mathbf{k}}\right) \cdot \left(\hat{\mathbf{g}}_x - j\hat{\mathbf{g}}_y\right) \end{aligned}. \tag{47}$$

Expanding with (12) and noting that $\hat{\mathbf{g}}'_x$ and $\hat{\mathbf{g}}'_y$ are defined to be orthogonal to $\hat{\mathbf{k}}$, we note $\hat{\mathbf{g}}'_x \cdot \hat{\mathbf{k}} = \hat{\mathbf{g}}'_y \cdot \hat{\mathbf{k}} = 0$, so

$$\begin{aligned} p &= \tfrac{C_g}{\sqrt{2}}\left(\hat{\mathbf{g}}'_x - j\hat{\mathbf{g}}'_y\right) \cdot \left(\hat{\mathbf{g}}_x - j\hat{\mathbf{g}}_y\right) \\ q &= \tfrac{C_g}{\sqrt{2}}\left(\hat{\mathbf{g}}'_x + j\hat{\mathbf{g}}'_y\right) \cdot \left(\hat{\mathbf{g}}_x - j\hat{\mathbf{g}}_y\right) \end{aligned}. \tag{48}$$

Expanding the product gives:

$$\begin{aligned} p &= \tfrac{C_g}{\sqrt{2}}\left(\hat{\mathbf{g}}'_x \cdot \hat{\mathbf{g}}_x - j\hat{\mathbf{g}}'_x \cdot \hat{\mathbf{g}}_y + j\hat{\mathbf{g}}'_y \cdot \hat{\mathbf{g}}_x + \hat{\mathbf{g}}'_y \cdot \hat{\mathbf{g}}_y\right) \\ q &= \tfrac{C_g}{\sqrt{2}}\left(\hat{\mathbf{g}}'_x \cdot \hat{\mathbf{g}}_x - j\hat{\mathbf{g}}'_x \cdot \hat{\mathbf{g}}_y - j\hat{\mathbf{g}}'_y \cdot \hat{\mathbf{g}}_x - \hat{\mathbf{g}}'_y \cdot \hat{\mathbf{g}}_y\right) \end{aligned}. \tag{49}$$

A subtle point here is that the dot product for complex numbers is equivalent to a conjugate transpose. With this equation, we can now take advantage of the property that each entry of a Rotation matrix is the dot product of a pair of unit basis vectors. Using this fact, we express the dot products in (49) as entries of the rotation matrix ${}^{G'_c}\mathbf{R}^{G_c}$.

$$\begin{aligned} p &= \tfrac{C_g}{\sqrt{2}}\left({}^{G'_c}\mathbf{R}^{G_c}_{xx} - j\,{}^{G'_c}\mathbf{R}^{G_c}_{xy} + j\,{}^{G'_c}\mathbf{R}^{G_c}_{yx} + {}^{G'_c}\mathbf{R}^{G_c}_{yy}\right) \\ q &= \tfrac{C_g}{\sqrt{2}}\left({}^{G'_c}\mathbf{R}^{G_c}_{xx} - j\,{}^{G'_c}\mathbf{R}^{G_c}_{xy} - j\,{}^{G'_c}\mathbf{R}^{G_c}_{yx} - {}^{G'_c}\mathbf{R}^{G_c}_{yy}\right) \end{aligned}. \tag{50}$$

The subscripts after each rotation matrix denote a particular entry, for instance the *xx* subscript in ${}^{G'_c}\mathbf{R}^{G_c}_{xx}$ represents the product of the *x*-basis vector in G'_c with the *x*-basis vector in G_c.

In this appendix, we consider a calibration that introduces no net LOS rotation ψ. As described in Section V (Calibration), we can use a Body ZYZ transformation for this purpose. For a Body ZYZ transformation, with Euler angles $\{\phi_1, \phi_2, \phi_3\}$, the relevant rotation matrix entries can be written [26]:

$$\begin{bmatrix} {}^{G'_c}\mathbf{R}^{G_c}_{xx} & {}^{G'_c}\mathbf{R}^{G_c}_{xy} \\ {}^{G'_c}\mathbf{R}^{G_c}_{yx} & {}^{G'_c}\mathbf{R}^{G_c}_{yy} \end{bmatrix} = \begin{bmatrix} -s_1 s_3 + c_1 c_2 c_3 & c_1 s_3 + s_1 c_2 c_3 \\ -s_1 c_3 - c_1 c_2 s_3 & c_1 c_3 - s_1 c_2 s_3 \end{bmatrix}. \tag{51}$$

Here where *s* and *c* are used as shorthand to indicate the sine and cosine functions. The subscript after *s* or *c* indicates one of the Euler angles. For instance, $s_3 = \sin(\phi_3)$.

To avoid introducing implicit spin about the LOS axis, we set $\{\phi_1, \phi_2\}$ equal to the Azimuth and Zenith angles $\{A_g, Z_g\}$, and then we choose $\phi_1 = -\phi_3 = -A_g$, as justified by Section V (Calibration). Simplifying to eliminate ϕ_3 from (51) gives

$$\begin{bmatrix} {}^{G'_c}\mathbf{R}^{G_c}_{xx} & {}^{G'_c}\mathbf{R}^{G_c}_{xy} \\ {}^{G'_c}\mathbf{R}^{G_c}_{yx} & {}^{G'_c}\mathbf{R}^{G_c}_{yy} \end{bmatrix} = \begin{bmatrix} s_1^2 + c_1^2 c_2 & c_1 s_1 (c_2 - 1) \\ c_1 s_1 (c_2 - 1) & c_1^2 + s_1^2 c_2 \end{bmatrix}. \tag{52}$$

Using this relationship between the rotation matrix and the Euler angles, we can rewrite (50) as

$$\begin{aligned} p &= \tfrac{C_g}{\sqrt{2}}(s_1^2 + c_1^2 c_2 + c_1^2 + s_1^2 c_2) \\ q &= \tfrac{C_g}{\sqrt{2}}\left(s_1^2 + c_1^2 c_2 - 2jc_1 s_1 (c_2 - 1) - (c_1^2 + s_1^2 c_2)\right) \end{aligned}. \tag{53}$$

Applying the identity that $(\sin^2\gamma + \cos^2\gamma) = 1$,

$$\begin{aligned} p &= \tfrac{C_g}{\sqrt{2}}(1 + c_2) \\ q &= \tfrac{C_g}{\sqrt{2}}(c_1^2 - 2jc_1 s_1 - s_1^2)(c_2 - 1) \end{aligned}. \tag{54}$$

In this expression, the first term in parentheses in q can be factored as $(c_1 - js_1)^2$ and converted into an exponential:

$$\begin{aligned} p &= \tfrac{C_g}{\sqrt{2}}(\cos\phi_2 + 1) \\ q &= \tfrac{C_g}{\sqrt{2}}(\cos\phi_2 - 1)e^{-2j\phi_1} \end{aligned}. \tag{55}$$

As a final step, we can show (55) is equivalent to (28) simply by substituting $\{\phi_1, \phi_2\}$=$\{A_g, Z_g\}$, as specified above.

Following the same procedure, it is straightforward to convert (27) into (29), completing the derivation.

APPENDIX B

This Appendix provides additional background on (30), which is drawn directly from the 14th equation of the seminal article by Wu [13]. To see the equivalence of (30) to the corresponding equation from [13], let us first consider the origins of (30). The spin angle between any pair of antennae for a given LOS can be determined by starting with both antennae pointing at each other, with boresights aligned with the LOS vector. In other words, the antenna basis vectors are aligned and the boresight vectors align with $\hat{\mathbf{k}}$. Define this case as the reference, with zero spin angle $\psi = 0$.

Next, the receiver and transmitter bases must be adjusted to arbitrary orientations relative to the inertial frame. In the process, the LOS vector $\hat{\mathbf{k}}$ remains fixed in the inertial frame while shifting to a new direction in each of the antenna frames. One way to re-orient the antennae is to use a combination of an LOS-

axis rotation followed by rotation about a carefully-selected orthogonal axis. For instance, to change the LOS vector in the receiver frame, rotate the receiver about the boresight by a first angle ϕ_z; then select a simple rotation axis $\hat{\boldsymbol{\lambda}}$ perpendicular to both the boresight and the desired LOS direction $\hat{\mathbf{k}}$. The first rotation (about the boresight $\hat{\mathbf{h}}_z$) induces spin; the second rotation about the $\hat{\boldsymbol{\lambda}}$ vector (orthogonal to both the boresight and LOS vectors) induces no spin. This pair of rotations, a Space Z rotation followed by a simple rotation, can place the receiver at any arbitrary orientation relative to the inertial frame. The transmit antenna can be rotated to an arbitrary orientation by a similar pair of rotations, starting with a rotation about the boresight (by θ_z) followed by a simple rotation that does not induce spin. Considering only geometric effects, the relative spin is influenced positively by the receiver and negatively by the transmitter. Thus, the total geometric spin is

$$\psi = \phi_z - \theta_z. \tag{56}$$

In order to relate this equation to (30), the pair of simple rotations described above must be converted to an equivalent set of three Euler angle rotations (e.g. a Body ZYZ rotation). Toward this objective, we note that the rotation matrix is a useful tool for comparison, since there is a unique rotation matrix for any relative orientation. Thus, we can compute the rotation matrix that describes the orientation of one antenna relative to the inertial frame, first using the twin simple rotations and subsequently using the triple Euler Angle (Body ZYZ) rotations. Noting the two rotation matrices are equivalent, we can relate the simple-spin angle ϕ_z to the receiver Euler angles $\{\phi_1, \phi_2, \phi_3\}$. The same process can be repeated for the transmitter to relate the simple-spin angle θ_z to the transmitter Euler angles $\{\theta_1, \theta_2, \theta_3\}$.

Start with the twin simple rotations for the receiver. The resulting rotation matrix between the final receiver orientation *H* and the initial (inertially-fixed) basis *N* is

$${}^{H}\mathbf{R}^{N} = \begin{bmatrix} \cos(\phi_z) & \sin(\phi_z) & 0 \\ -\sin(\phi_z) & \cos(\phi_z) & 0 \\ 0 & 0 & 1 \end{bmatrix} \mathbf{R}(\gamma, \boldsymbol{\lambda}). \tag{57}$$

On the left-hand side, the first matrix is a space rotation about the boresight $\hat{\mathbf{h}}_z$ axis and the second is the simple rotation matrix for a rotation of angle γ about a unit vector $\boldsymbol{\lambda}$ such that

$$\boldsymbol{\lambda} = \hat{\mathbf{h}}_z \times \hat{\mathbf{k}} \,/\, \left\| \hat{\mathbf{h}}_z \times \hat{\mathbf{k}} \right\|. \tag{58}$$

This equation implies the vector $\boldsymbol{\lambda}$ is perpendicular to both the boresight $\hat{\mathbf{h}}_z$ and the LOS vector $\hat{\mathbf{k}}$. The form of the simple rotation matrix is given in many advanced dynamics and robotics textbooks, such as for example in [26]. Note that there is a special case when the rotation angle γ is zero; in this case, (58) is singular but does not need to be computed, since the rotation matrix $\mathbf{R}(\gamma, \boldsymbol{\lambda})$ is simply the identity matrix.

Proceeding with the nontrivial case, let us expand (57) by matrix multiplication. Then extract individual elements of the resulting rotation matrix. First consider the [3,3] element, which is the lowest diagonal element:

$${}^{H}\mathbf{R}^{N}[3,3] = \cos(\gamma). \tag{59}$$

Summing the other two diagonal elements gives:

$$R_{sum} = {}^{H}\mathbf{R}^{N}[1,1] + {}^{H}\mathbf{R}^{N}[2,2] \tag{60}$$

with

$$R_{sum} = \cos(\phi_z)\Big(\big(1-\cos(\gamma)\big)\big(\lambda_x^2 + \lambda_y^2\big) + 2\cos(\gamma)\Big). \tag{61}$$

Here λ_x and λ_y are the coefficients of the simple rotation vector about the inertially-fixed x and y axes. The third measure describing the simple rotation vector is $\lambda_z = \boldsymbol{\lambda} \cdot \hat{\mathbf{k}}$. Note from (58) that the cross product makes $\boldsymbol{\lambda}$ orthogonal to $\hat{\mathbf{k}}$, such that $\lambda_z = 0$. Furthermore, because (58) is normalized to ensure that $\boldsymbol{\lambda}$ is a unit vector, then $\big(\lambda_x^2 + \lambda_y^2 + \lambda_z^2\big) = \big(\lambda_x^2 + \lambda_y^2\big) = 1$. Hence:

$$R_{sum} = \cos(\phi_z)\big(1 + \cos(\gamma)\big). \tag{62}$$

Finally, consider the difference of two more rotation-matrix elements, the first two off-diagonal terms:

$$R_{diff} = {}^{H}\mathbf{R}^{N}[2,1] - {}^{H}\mathbf{R}^{N}[1,2] \tag{63}$$

with

$$R_{diff} = \sin(\phi_z)\Big(\big(1-\cos(\gamma)\big)\big(\lambda_x^2 + \lambda_y^2\big) + 2\cos(\gamma)\Big), \tag{64}$$

which, noting that $\big(\lambda_x^2 + \lambda_y^2\big) = 1$, simplifies to

$$R_{diff} = \sin(\phi_z)\big(1 + \cos(\gamma)\big). \tag{65}$$

The rotation matrix ${}^{H}\mathbf{R}^{N}$ can equivalently be computed from a set of three Body ZYZ Euler angles $\{\phi_1, \phi_2, \phi_3\}$. This form of the rotation matrix is also tabulated in standard dynamics textbooks, such as [26]. Using this table, we can write the rotation matrix elements in terms of the Euler angles as

$${}^{H}\mathbf{R}^{N}[3,3] = \cos(\phi_2) \tag{66}$$

and

$$R_{sum} = \cos(\phi_1 + \phi_3)\big(1 + \cos(\phi_2)\big) \tag{67}$$

and

$$R_{diff} = \sin(\phi_1 + \phi_3)\big(1 + \cos(\phi_2)\big). \tag{68}$$

It is now possible to match the coefficients of the rotation matrix obtained from (57) with the Body ZYZ coefficients. Matching (59) and (66), we have

$$\cos(\gamma) = \cos(\phi_2). \tag{69}$$

Now matching the R_{sum} expressions of (62) and (67), then substituting (69), we have

$$\cos(\phi_z) = \cos(\phi_1 + \phi_3). \tag{70}$$

Similarly by matching the R_{diff} expressions of (65) and (68), then substituting (69), we have

$$\sin(\phi_z) = \sin(\phi_1 + \phi_3). \tag{71}$$

By inspection from (70) and (71), and restricting the arguments of the trigonometric functions to be on the range 0 to 2π, we see

$$\phi_z = \phi_1 + \phi_3. \tag{72}$$

In short, the spin angle ϕ_z of the receiver relative to the inertial orientation is equivalent to the sum of the first and third Euler angle, ϕ_1 and ϕ_3, in the Body ZYZ rotation. Normally, it is dangerous to sum Euler angles that describe a three-dimensional rotation [26]; however, in this case, we have a mathematical justification to sum the first and third Body ZYZ Euler angles to compute the receiver spin ϕ_z relative to its initial orientation.

Following the same approach for the transmitter, we can show the parallel result, which is that

$$\theta_z = \theta_1 + \theta_3. \tag{73}$$

Substituting both (72) and (73) into (56), we recover (30).

$$\psi = \phi_1 + \phi_3 - \theta_1 - \theta_3. \tag{30}$$

The goal of this supplement was not only to derive (30), but also to relate it to the 14th equation of Wu. To do this, consider the relative angle $\phi_3 - \theta_3$ in (30), which is defined in this paper to be a difference of the third Body ZYZ Euler angles used to generate the bases $\{\hat{\mathbf{g}}'_x, \hat{\mathbf{g}}'_y, \hat{\mathbf{k}}\}$ and $\{\hat{\mathbf{h}}'_x, \hat{\mathbf{h}}'_y, \hat{\mathbf{k}}\}$. The angle difference represents a relative rotation about $\hat{\mathbf{k}}$, which can be computed from the basis vectors using (44) and (45). Substituting (44) into (30) gives

$$\psi = \phi_1 + \psi^* - \theta_3, \tag{74}$$

where

$$\psi^* = \text{sign}\left(\hat{\mathbf{k}} \cdot \left(\hat{\mathbf{g}}'_y \times \hat{\mathbf{h}}'_y\right)\right) \text{acos}\left(\hat{\mathbf{g}}'_y \cdot \hat{\mathbf{h}}'_y\right). \tag{45}$$

Equation (74) recovers Wu's equation with one exception. The exception is the negative sign in the θ_1 term of (74). This negative sign can be reconciled by noting that [13] defines the receiver azimuth angle about an axis opposite to that used in this paper. The different basis convention used in this paper ensures that the antenna bases align when the receiver and transmitter point at each other (not true for [13]). Correcting for the opposite orientations of the receiver boresight axes between papers, we see that (74) from this paper is indeed equivalent to the 14th equation of Wu.

REFERENCES

[1] Banville, S., Santerre, R., Cocard, M., and R.B. Langley, "Satellite and receiver phase bias calibration for undifferenced ambiguity resolution," *Proc. ION National Technical Meeting (NTM)*, San Diego, CA, 2008, pp. 711-719.

[2] Kim, D., Serrano, L., and Langley, R., "Phase Wind-Up Analysis-Assessing Real-Time Kinematic Performance," *GPS World*, Vol. 17, No. 9, 2006, pp. 58-64.

[3] Kechine, M., Tiberius, C., and Van Der Marel, H., "Network differential GPS: kinematic positioning with NASA's internet-based global differential GPS," *J. Global Positioning Systems*, Vol. 2, No. 2, 2003, pp. 139-143.

[4] Soltz, J.A., "Attitude determination of a rotating body using INS and GPS data," *AIAA Guidance, Navigation, and Control Conference*, Scottsdale, AZ, 1994, pp. 1223-1233.

[5] Psiaki, M.L., and Mohiuddin, S., "Modeling, analysis, and simulation of GPS carrier phase for spacecraft relative navigation," *J. Guidance, Control, and Dynamics*, Vol. 30, No. 6, 2007, pp. 1628-1639.

[6] Axelrad, P., and Behre, C.P., "Attitude estimation algorithms for spinning satellites using global positioning system phase data," *J. Guidance, Control, and Dynamics*, Vol. 20, No. 1, 1997, pp. 164-169.

[7] Lightsey, E.G., "Method for attitude determination using GPS carrier phase measurements from nonaligned antennas," U.S. Patent No. 6,005,514, issued December 21, 1999.

[8] Dong, D., Chen, W., Cai, M., Zhou, F., Wang, M., Yu, C., Zheng, Z., and Wang, Y., "Multi-antenna synchronized global navigation satellite system receiver and its advantages in high-precision positioning applications," *Frontiers of Earth Science*, Vol. 10, No. 4, 2016, pp. 772-783.

[9] García-Fernández, M., Markgraf, M., and Montenbruck, O., "Spin rate estimation of sounding rockets using GPS wind-up," *GPS Solutions*, Vol. 12, No. 3, 2008, pp. 155-161.

[10] Pei, C., "Attitude determination algorithms for spinning satellites using single antenna GPS receiver and MEMS gyro," *Aerospace Science and Technology*, Vol. 26, No. 1, 2013, pp.10-15.

[11] Chiang, K., Psiaki, M., Powell, S., Miceli, R., & O'Hanlon, B., "GPS-based attitude determination for a spinning rocket," *IEEE Transactions on Aerospace and Electronic Systems*, Vol. 50, No. 4, 2014, pp. 2654-2663.

[12] Weaver, B., Bogner, T., Soltz, J.A., and Rife, J., "GPS-based attitude determination of a rotating body using single-antenna subject to phase wind-up," in *Proc. ION Global Navigation Satellite Systems+* (ION GNSS+), Miami, FL, 2019, pp. 1164 - 1171.

[13] Wu, J. T., Wu, S. C., Hajj, G. A., Bertiger, W. I., and Lichten, S. M., "Effects of antenna orientation on GPS carrier phase," in *AAS/AIAA Astrodynamics Conference*, Durango, CO, 1991.

[14] Beyerle, G., "Carrier phase wind-up in GPS reflectometry," *GPS solutions*, Vol. 13, No. 3, 2009, pp. 191-198.

[15] Burke, G. J., Poggio, A.J., Logan, J.C., and Rockway, J.W., "Numerical electromagnetic code (NEC)," in *1979 IEEE International Symposium on Electromagnetic Compatibility*, IEEE, 1979, with open-source code hosted at http://www.nec2.org/.

[16] Stutzman, W.L., and Thiele, G.A., *Antenna theory and design*, Wiley, 2012.

[17] Chryssomallis, M., and Christodoulou, C. "Antenna radiation patterns," *Wiley Encyclopedia of Electrical and Electronics Engineering*, Wiley, 1999.

[18] Rothacher, M., Schaer, S., Mervart, L., and Beutler, G, "Determination of antenna phase center variations using GPS data," in *Proc. IGS Workshop on Special Topics and New Directions*, Potsdam, Germany, 1995, pp. 205-220.

[19] van Graas, F., Bartone, C., Arthur, T., "GPS antenna phase and group delay corrections," in *Proc. ION National Technical Meeting* (ION NTM), San Diego, CA, 2004, pp. 399-408.

[20] Wübbena, G., Schmitz, M., Boettcher, G., and Schumann, C., "Absolute GNSS antenna calibration with a robot: repeatability of phase variations, calibration of GLONASS and determination of carrier-to-noise pattern," in *Proceedings of the IGS Workshop*, Darmstadt, Germany, 2006.

[21] Kim, U.-S. *Mitigation of signal biases introduced by controlled reception pattern antennas in a high integrity carrier phase differential GPS system*, PhD Dissertation, Stanford University Dept. Aeronautics and Astronautics, 2007.

[22] Church, C. M., O'Brien, A. J., and Gupta, I.J., "A novel method to measure array manifolds of GNSS adaptive antennas," *NAVIGATION*, Vol. 58, No. 4, 2011, pp. 345-356.

[23] De Lorenzo, D. S., Lo, S. C., Enge, P. K., and Rife, J., "Calibrating adaptive antenna arrays for high-integrity GPS," *GPS solutions*, Vol. 16, No. 2, 2012, pp. 221-230.

[24] Caizzone, S., Circiu, M.-S., Elmarissi, W., Enneking, C., Felux, M., Yinusa, K., "Antenna influence on Global Navigation Satellite System pseudorange performance for future aeronautics multifrequency standardization," *NAVIGATION*, Vol. 66, No. 1, 2019, pp. 99-116. https://doi.org/10.1002/navi.281

[25] Misra, P., and Enge, P., *Global Positioning System: signals, measurements and performance second edition*, Ganga-Jamuna Press, 2006.

[26] Mitiguy, P. *Advanced Dynamcis and Motion Simulation: for Professional Engineers and Scientists*, MotionGenesis, 2019.

[27] Trimble, "Basics of GPS and RTK: Antenna phase centers," Accessed on: December 2, 2019. [Online]. Available: https://www.trimble.com/OEM_ReceiverHelp/V4.44/en/AntennaPhaseCenters.html

BIOGRAPHIES

Jason H. Rife (M'01) received his B.S. in mechanical and aerospace engineering from Cornell University, Ithaca, NY, and his M.S. and Ph.D. in mechanical engineering from Stanford University, Stanford, CA.

He is currently an Associate Professor of Engineering at Tufts University in Medford, MA. At Tufts, he directs the Automation Mechanical Safety and Robotics Laboratory (ASAR), which applies theory and experiment to characterize the integrity of autonomous vehicle systems.

Brandon M. Weaver received his Bachelor of Mechanical Engineering from Auburn University, Auburn, AL. He has worked for The Charles Stark Draper Laboratory, Inc. where he evaluated GPS receiver performance under adverse conditions.

He is currently a Draper Fellow working towards his M.S in mechanical engineering at Tufts University, Medford, MA. He is currently researching attitude determination methods using GPS carrier phase measurements.

Anthony Bogner received his B.S. in aerospace engineering from Texas A&M University, College Station, TX, and his M.S. in Aeronautics and Astronautics from the Massachusetts Institute of Technology, Cambridge, MA.

He is currently a staff engineer at Draper in the Autonomy, Guidance and Control Division. He supports the integration of GPS into vehicle navigation systems.

J. Arnold Soltz has a B.A. from Johns Hopkins University (1964) and an M.S. from Northeastern University (1969).

He is a principal member of the technical staff at Draper with over 40 years of experience in the design, implementation, and verification of the models of signals, sensors, and systems used for navigation in spacecraft, aircraft, terrestrial surveying, and undersea vehicles. He is a member of the Institute of Navigation (ION).